Journal of Materials Chemistry C

Accepted Manuscript

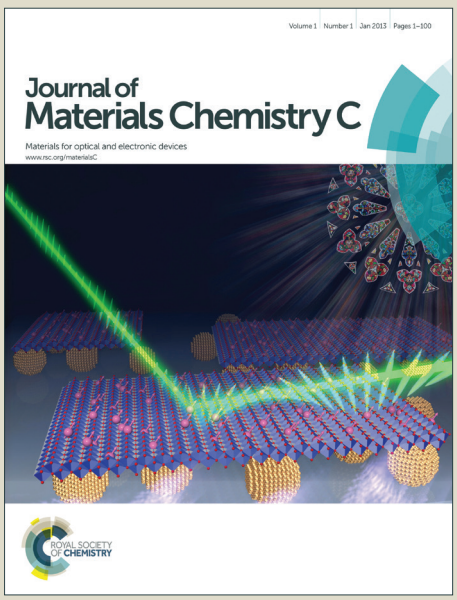

ROYAL SOCIETY OF CHEMISTRY

www.rsc.org/materialsC

Journal Name

RSCPublishing

ARTICLE

Atomic Layer Deposition of Zinc Oxide onto and into P3HT for Hybrid Photovoltaics

Cite this: DOI: 10.1039/xoxxoooooox

S. Obuchovsky,[a] I. Deckman[a], M. Moshonov[a], T. Segal-Peretz[a], G. Ankonina[b], T. J. Savenije[c], and G. L. Frey[a].

Received ooth January 2012,
Accepted ooth January 2012

DOI: 10.1039/xoxxoooooox

www.rsc.org/

Hybrid organic-inorganic bulk heterojunction (BHJ) photovoltaic devices continue to be a promising alternative for present semiconductor solar cell technology. However, to become competitive hybrid devices must improve their currently low efficiencies. A major challenge to overcome is the control over the hybrid morphology, and more specifically, directing interpenetrated nano-scale phase separated continuous networks through the active layer. Here we demonstrate that atomic layer deposition (ALD) can be used to deposit hybrid BHJ photovoltaic films with exceptional control over film composition and morphology. The BHJ is prepared by exposing a pre-formed conjugated polymer film to an ALD alternating sequence of a metal oxide precursor and water. In this study ZnO was grown from cycles of diethyl zinc (DEZ) and water inside pre-formed P3HT films. We find that DEZ diffuses into the amorphous regions of the P3HT film, followed by oxidation by water to form ZnO crystalline particles (5-10 nm). Importantly, the inorganic crystalline phase is formed within the polymer amorphous regions while the ordered polymer domains are maintained. Investigation of the growth mechanism and control over the number of ALD cycles allowed us to direct a BHJ morphology with: I) a continuous ZnO network through the P3HT film; II) a descending concentration gradient of ZnO from the top surface down to the substrate; and III) a dense ZnO electron transporting layer on the polymer film surface. The successful morphology-control is manifested in efficient photocurrent generation, evident from time resolved microwave-photoconductivity measurements and device performances that are similar to those reported for intensely optimized conjugated polymer/metal oxide solar cells.

Introduction

Organic photovoltaic devices (OPV) have the potential to become a leading alternative source for renewable energy with the advantages of low cost processing, flexibility and versatility [1, 2]. The optimal device morphology is a bulk heterojunction (BHJ) where charge generation is enhanced by the high interfacial area and charge transport is supported by the continuous pathways of each component to the respective electrode. Consequently, the device performance critically depends on the phase separation and film morphology which are challenging to control due to their sensitivity to preparation and operation conditions.[1, 3-5] Alternative promising systems are hybrid organic/inorganic photovoltaic devices (HOPVs) consisting of an inorganic acceptor network embedded in a conjugated polymer donor matrix. Such systems still exploit the advantages of organic electronics, but also offer enhanced electron conductivity, improved chemical stability and better morphological control endowed by the inorganic component.[3, 6]

Most commonly used inorganic acceptors for HOPV are metal oxides, specifically TiO_2[7, 8] and ZnO.[3, 9] Several methodologies have been used to prepare hybrid BHJs. The first method generally involves a two-step processing sequence: initially nano-scale metal oxide structures such as nanoparticles,[10] nanorods[11, 12] or a mesoporous network[13] are prepared, followed by spin coating of the polymer onto the preformed inorganic structures. However, the mismatch between the chemical nature of the components hinders the organic phase infiltration into the inorganic nanostructure[14]. Alternatively, an organometallic metal oxide precursor is added to the polymer solution followed by simultaneous casting and *in-situ* conversion of the precursor to the metal oxide inside the polymer film. However, these processing conditions limit the control over the nano-scale donor/acceptor morphology and the interfacial intimacy.[6, 8, 15]

An alternative technique for the deposition of metal oxides is Atomic Layer Deposition, ALD. In general, ALD is used to grow conformal metal oxide coatings on -OH and $-NH_2$ terminated surfaces using sequential, self-limiting reactions of a reactive organometallic precursor and an oxidizing agent.[16, 17] Accordingly, Moghaddam et al. end-functionalized poly(3-hexylthiophene-2,5-diyl), P3HT, with acid carboxylic groups to serve as reactive sites for the growth of ZnO sheets.[18] Interestingly, attempts to deposit Al_2O_3 using ALD on polymer films with CH3 termination, such as polyethylene and polystyrene, revealed that the absence of the reactive groups on the

surface lead to the diffusion of the organometallic precursor into the polymer film and its *in-situ* conversion to the inorganic cluster.[19] These results inspired us to suggest the general use of ALD for the deposition metal oxide networks inside conventional conjugated polymer films.

In this report we show a new and general approach for processing HOPVs using ALD which does not require chemical modifications of the conjugated polymer host and is not limited to polymer films with preferable precursor reaction sites. The generality of the approach is demonstrated ALD of a ZnO network from DEZ and water precursors inside the most commonly used pristine P3HT. Moreover, we show that the different deposition sequences of these precursors can be used to control the desired organic/inorganic BHJ morphology and to produce hybrid films with homogenous lateral metal oxide distribution throughout the organic layer. Finally, we integrate the ALD processed BHJ as active layers in photovoltaic devices and show that the control over the deposition parameters is manifested in the photovoltaic performance. These results establish that ZnO deposition via ALD is a promising technique for processing hybrid BHJ morphologies.

Experimental

1,2-dichlorobenzene (DCB) and diethylzinc (DEZ, cylinder-packaged for use in ALD deposition systems) were purchased from Aldrich and used as received. Poly(3-hexylthiophene-2,5-diyl) (P3HT, Mw=50,000 gr/mol, 95% regioregularity) was purchased from Reike Metals, Inc. U.S.A and used as-received. An aqueous dispersion of poly(3,4-ethylendioxythiophene)-poly(styrenesulfonate) (PEDOT:PSS), was acquired from Haraeus (CLEVIOSTM P VP AL 4083) and was filtered through a 0.45µm PTFE filter before use.

Substrates used in this study include quartz, silicon and ITO covered glass. All substrates were cleaned thoroughly by sonication in acetone, methanol and isopropanol for 15 min each. For devices ITO substrates were held in ozone atmosphere for 15 min prior to spin coating a PEDOT:PSS solution, followed by a heat treatment on a hot plate for 15 min at 100°C.

150 nm-thick P3HT films were spun from a 37 mg/ml DCB solution at 1000 RPM for 120 seconds under ambient conditions, the coating was followed by an annealing treatment at 170°C for 1 hour (heating rate of 3°C /min) in vacuum in order to enhance crystallization and ensure complete solvent outgassing. ZnO was ALD deposited in an Applied Microstructures MVD100E system with an integrated oxygen plasma module. Deposition temperature was set to 60°C and alternating 1 torr pulses of DEZ and water were applied. The precursor reaction time was limited to 1 sec for both DEZ and water in every cycle. The reaction chamber was purged with nitrogen between different precursor pulse injections.

Device fabrication was completed by thermal evaporation of a 95 nm-thick Al layer on glass/ITO/PEDOT:PSS/P3HT:ZnO films, followed by post-evaporation annealing for 5 min at 100°C in an N_2 atmosphere. Current-density–voltage (J–V) curves were measured under 100 mW/cm^2 AM 1.5G illumination (Newport Inc. 67005 150W Xe arc lamp solar simulator) using a Keithley 2400 source-meter.

Optical absorbance measurements of films on quartz were performed using a Varian Cary 100 Scan UV-Vis spectrophotometer in the 250-800 nm range. Grazing incidence X-ray diffraction (GIXRD) measurements (ω=3°) of films on silicon substrates were conducted on a D/MAX-2500 series, RIGAKU system with Cu Kα radiation (λ = 1.5418 Å). Scanning electron microscopy (HRSEM) micrographs of films on silicon were acquired using a Zeiss Ultra-Plus FEG-SEM operating at 2 KeV and the EDS measurements were conducted at a 4KeV operating voltage. EDS measurements include Kα signals of sulfur, carbon and oxygen as well as the Lα signal of zinc. The Si (substrate) signal was observed in all EDS measurements to ensure that the interaction volume was larger than the film thickness. High-resolution transmission electron microscopy (HRTEM) micrographs of films on Si were acquired using a FEI Titan 80-300 KeV FEG-S/TEM operating at 200 KeV. Cross section samples for HRTEM examination were done using a Focused Ion Beam integrated in the Strata 400 STEM Dual Beam system of a Field-Emission Scanning Electron Microscope (FE-SEM).

Photoconductance measurements on the P3HT:ZnO films were carried out using the photo-induced time-resolved microwave conductance (TRMC) technique. This technique was previously used to study the charge transport properties in a wide range of materials including organic and hybrid organic inorganic blend films.[20-24]. Briefly, a quartz substrate with the active layer is mounted in a home-built, sealed X-band (8.4 GHz) microwave cell filled with N_2. The activelayer is then photo-excited with a 3 ns laser pulse from an optical parametric oscillator pumped by a Q-switched Nd:YAG laser (Vibrant II, Opotek) operating at 10 Hz. The overall response time of the setup, including the electronics used for detection, is ~18 ns.

Photo-excitation of the active layer results in the generation of mobile charge carriers effectively modulating its conductance (ΔG). Because there are no electrodes, the photo-generated charges decay with time via recombination and/or trapping processes. The change in conductance with time (ΔG(t)) results in a variation of the normalized reflected microwave power (ΔP(t)/P) from the loaded cell and is given by:[25]

$$\frac{\Delta P(t)}{P} = -K\Delta G(t) \qquad (1)$$

where K represents a sensitivity factor that is determined from the dimensions of the microwave cell and the geometrical properties of the media in the microwave cell. The time-dependent change in conductance (ΔG(t)) can be expressed in terms of the yield of photo-induced electrons and holes (φ) and the sum of their mobilities (Σμ). If the decay of the photo-induced charges is longer than the time resolution of the detection system, then the maximum change in conductance (ΔG_{max}) with respect to the incident light yields the following equation:[25]

$$\varphi \sum_i \mu_i = \frac{\Delta G_{\max}}{\beta e I_o F_A} \qquad (2)$$

Here, I_0 is the incident light intensity per pulse and FA is the fraction of incident photons absorbed, β is the ratio between the broad and narrow internal dimensions of the microwave cell and *e* is the electron charge.

Results and discussion

The feasibility of metal oxide deposition into P3HT by ALD was first examined on relatively thick films of 0.5 µm to establish the diffusion viability and penetration depth. Figure 1A shows a back scattering (BSE) HRSEM cross section image of the P3HT film after

100 alternating cycles of DEZ and water. The bright domains represent the higher density nanoparticles dispersed in the P3HT matrix (dark contrast). The image clearly shows a descending concentration gradient of the nanoparticles down to the substrate, and a uniform continuous dense layer on the P3HT surface.

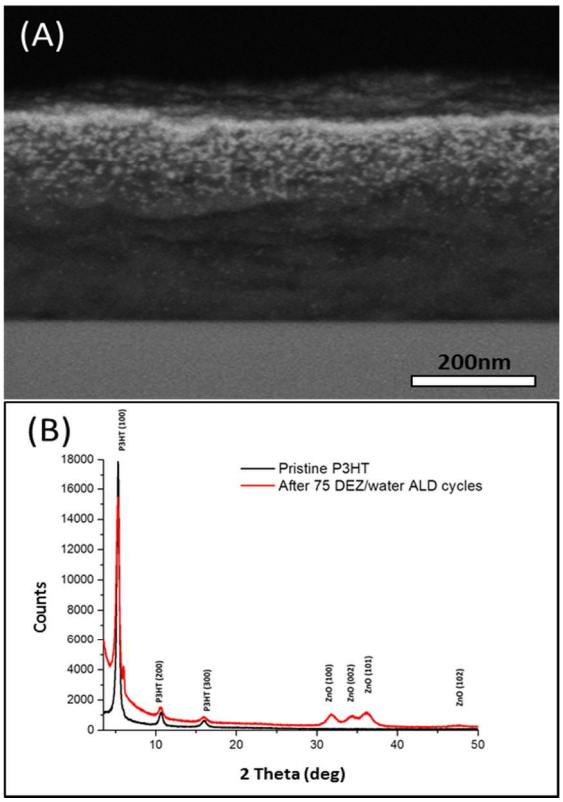

Figure 1: (A) Cross section BSE HRSEM micrograph of a P3HT film on a silicon substrate, after 100 ALD alternating cycles of DEZ and water. (B) GIXRD patterns of a pristine P3HT film before (black line) and after 75 DEZ/water ALD cycles (red line).

Grazing incidence Xray diffraction (GIXRD) was performed on films prior and post the ALD sequence to characterize the particles deposited in the P3HT film. The GIXRD pattern of pristine P3HT (black line in Figure 1B), shows three peaks corresponding to the (100), (200), (300) reflections associated with the 1.6 nm lamellar distance typical in crystalline P3HT domains.[11] Previous studies reported that ALD alternating cycles of DEZ and water ALD, even at relatively low temperatures <200 °C, results in the deposition of highly crystalline ZnO wurtzite with little to no hydroxides and/or amorphous regions.[26] Indeed, GIXRD patterns after the ALD process show four new peaks, all in very good agreement with the first four wurtzite reflections of ZnO (red line in Figure 1B).[27] Furthermore, signals associated with a $Zn(OH)_2$ phase are not observed in the GIXRD pattern. The general increase of the background signal after the ALD process (low angle range) is due to the increased total reflection from the higher density ZnO-rich sample surface.[28] Therefore, the GIXRD results demonstrate that a simple ALD process of DEZ and water pulse sequence results in the successful deposition of nanocrystalline ZnO particles inside the P3HT film.

The morphology and crystallinity of the ZnO particles is also evident from the cross section bright filed TEM micrographs in Figure 2. In these images, the darker contrast represents the denser ZnO-rich areas and the bright contrast is the P3HT matrix. The low magnification image, Figure 2A, shows ZnO-rich areas dispersed throughout the hybrid film reaching down to the substrate with a descending concentration gradient. In the high magnification micrograph, Figure 2B, the lattice image and typical size of individual ZnO nanoparticles, 5 to 10 nm, are identified. The selected area FFT analysis shows distinct diffraction spots in a circle-like pattern, Figure 2 inset, confirming that the ZnO particles are crystalline and suspended in the film with no preferred orientation. The crystallinity of the ZnO particles is also apparent from the presence of an optical transition at ~350 nm in the optical absorption spectra of all films exposed to the ALD cycling (Figure 3A). This transition corresponds to the optical bang gap of ZnO, [29] and increases with the number of ALD cycles. Importantly, the agglomerated ZnO nanocrystals form a pseudo-interconnected network through the film which would be able to support charge transport in a corresponding photovoltaic device[2].

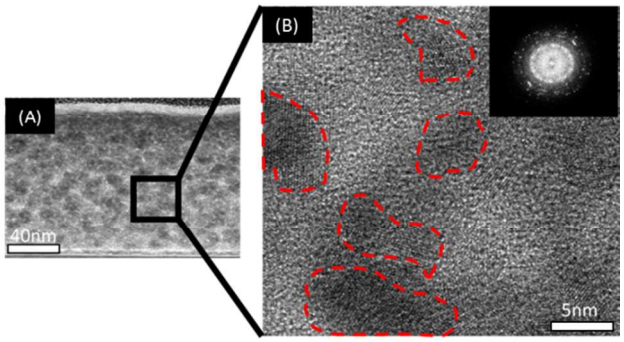

Figure 2: Low (A) and high (B) magnification cross section bright filed TEM micrographs of a P3HT film on a silicon substrate 75 DEZ/water ALD cycles. Inset: the corresponding FFT analysis.

The penetration of DEZ into the P3HT film followed by its *in-situ* conversion to ZnO could potentially reduce the crystallinity of P3HT and/or its conjugation length, which in turn would reduce the hole conductivity and light absorption in a corresponding photovoltaic device.[30] The effect of ZnO deposition on the P3HT host was studied by comparing the absorption spectra of the films before and after the ALD process. Figure 3A shows that all absorption spectra measured after the different ALD processes include the typical P3HT intra-molecular vibronic transitions, at 518 and 552 nm; and the shoulder at 605 nm, indicative of ordered P3HT domains.[31] Yet, a closer look at the absorption spectra reveals that the polymer chain's morphology is slightly affected by the ZnO incorporation. This effect becomes evident by normalizing the data in Figure 3A to resolve the changes in the location and breadth of the P3HT transitions (Figure 3B). A minor broadening of the P3HT spectra to higher energies with increased ALD cycles (red arrow in Figure 3B) implies a somewhat shorter average conjugation length.[32] Moreover, after the extensive deposition sequences of 75 and 100 cycles, the intensity of the 605 nm transition is slightly reduced (black arrow in Figure 3B) associated with only a minor decrease in P3HT order. The small effect of ZnO deposition on the P3HT ordered domains could indicate that the ZnO deposition occurs selectively in the amorphous regions of the semicrystalline P3HT. We speculate that the DEZ diffuses into the amorphous regions followed by their *in-situ* conversion to ZnO. These results demonstrate that, in contrast to all other processing methods, ALD can be used to introduce the ZnO particles within the disordered domains with little to no deterioration of the P3HT crystallinity and optical properties.

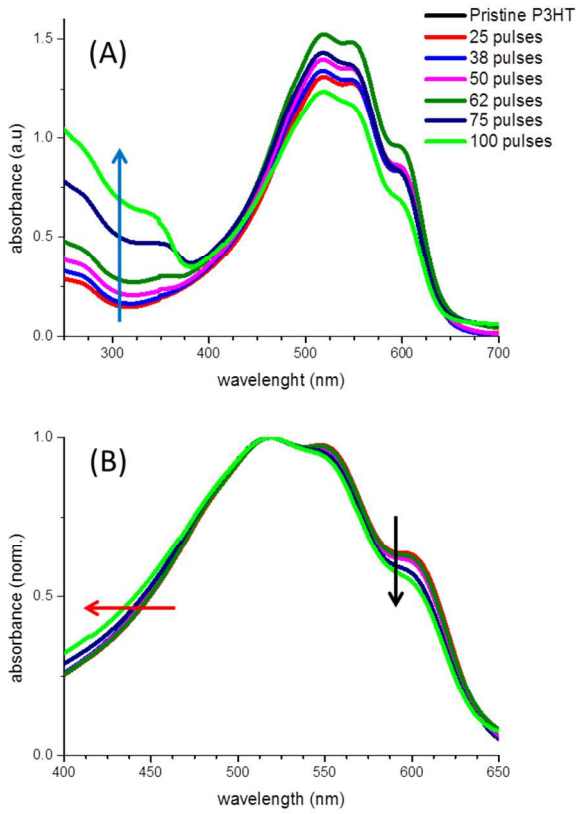

Figure 3: As is (A), and normalized (at 518 nm) (B), absorbance spectra of P3HT films subjected to DEZ/water cycles: Black- pristine P3HT, red – 25 cycles, blue- 38, magenta- 50, olive- 62, navy- 75, green- 100

After confirming that ALD can be used to deposit crystalline ZnO nanoparticles inside P3HT films, we studied the growth mechanism to allow the correlation between the deposition process and the final film morphology. To do so we compared the cross sections HRSEM images of P3HT films subjected to a variety of DEZ/water ALD cycles, as shown in Figure 4. The images clearly show a strong correlation between the number of cycles and the volume fraction of ZnO in the film. More specifically, after 25 ALD cycles (Figure 4A) there is no clear evidence of ZnO in the organic film, in a good agreement with the optical measurements (Figure 3A). However, after 38 ALD cycles initial ZnO spots are noticed evenly distributed throughout the film (Figure 4B). The number and size of the ZnO particles is increased after 50 cycles (Figure 4C). Notably, as the deposition progresses the particles at the polymer surface grow and finally merge into a continuous ZnO layer covering the top of the P3HT film (Figure 4 D, E and F).

The growth mechanism of ZnO by ALD from DEZ/water alternating cycles onto OH terminated surfaces is widely studied and well established. The accepted mechanism suggests that the substrate's surface hydroxyl groups act as nucleation sites for the first DEZ pulse according to the reaction shown in equation 3. The following exposure to water results in substitution of the ethyl group (equation 4) and re-generation of a hydroxyl rich surface. Repeating the successive DEZ and water cycles, therefore, leads to the self-limiting layer-by-layer growth of a ZnO film.[33]

$$\text{Sub-OH} + C_2H_5ZnC_2H_5 \rightarrow \text{Sub-O-Zn}C_2H_5 + C_2H_6 \quad (3)$$

$$\text{Sub-O-Zn}C_2H_5 + H_2O \rightarrow \text{Sub-O-Zn-OH} + C_2H_6 \quad (4)$$

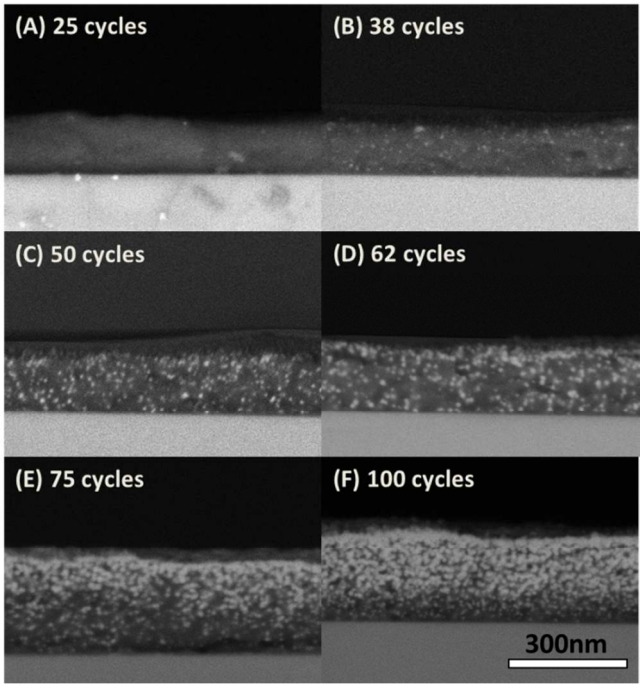

Figure 4: Cross section BSE HRSEM micrographs of P3HT films after 25, 38, 50, 62, 75, 100 DEZ/water ALD cycles.

However, this simple mechanism is unsuitable for describing the ALD growth of metal oxides onto polymer surfaces. In the study by Wilson et al.[19] attempts to ALD deposit a uniform Al_2O_3 coating onto polymer films resulted in metal oxide growth inside the polymer films. It was suggested that due to the lack of the precursor-surface reaction, the metal oxide precursor diffuses into the organic layer, followed by a sequential reaction with water inside the film. We suggest that the lack of reactive hydroxyl groups on the P3HT surface also results in DEZ diffusion into the polymer film. In the next step, the P3HT film that retained some of the DEZ molecules is exposed to a water pulse. Although the film is originally highly hydrophobic, several studies have reported the diffusion of organic molecules varying in hydrophobicity through conjugated organic films.[34-37] Very recently Friend et al. reported the diffusion of methanol through a 200 nm all-organic BHJ down to the PEDOT:PSS layer. In addition, the high reactivity of the DEZ and water reaction further encourages water diffusion into the P3HT towards the incorporated DEZ molecules. The diffusing water molecules react with the retained DEZ in the P3HT film forming the primary ZnO clusters (Figure 4B). Successive alternating DEZ and water cycles generate additional ZnO clusters inside the P3HT (Figure 4C). At a certain stage, particle growth is faster than particle nucleation because growth requires the diffusion of one precursor only, either DEZ or water, while nucleation requires the diffusion of both (Figure 4D). Importantly, due to this growth mechanism, the ZnO particles close to the polymer surface grow faster than those that are embedded deeper in the polymer film. Therefore, after extensive cycling a continuous ZnO layer fully covers the P3HT surface. This ZnO layer now acts as a substrate for the conventional

self-limiting layer-by-layer growths described above for surfaces and described in equation 3 and 4 (Figures 4 E and F).

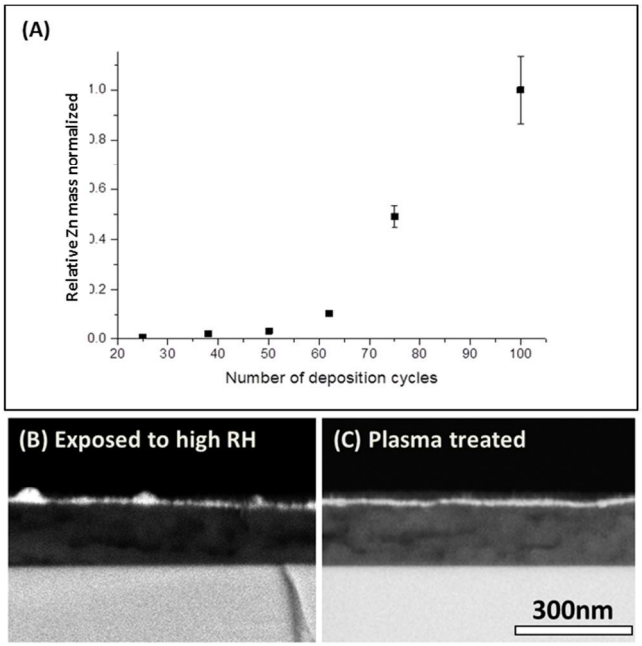

Figure 5: (A) The Zn/S wt% ratio after 25, 38, 50, 62, 75, 100 DEZ/water deposition cycles calculated from the EDS measurements. (B, C) Cross section BSE HRSEM micrographs of pre-treated P3HT films after 75 DEZ/water deposition cycles. (A) The P3HT film was exposed to high humidity prior to the ALD process. (B) P3HT film was exposed to an oxygen plasma treatment prior to the ALD process.

The suggested mechanism was corroborated using SEM EDS measurements by calculating the ZnO mass accumulation as a function of the number of ALD cycles. Because the P3HT layer thickness was identical for all films, the total mass of sulfur was regarded identical and constant in all films. The total mass of Zn, on the other hand, increases with the number of cycles and, assuming full DEZ conversion, represents the mass accumulation of ZnO. Under such conditions, the Zn/S wt% ratio evaluated from the EDS Kα signal of sulfur and Lα signal of zinc, is proportional to the total mass of zinc in each film. For presentation means the calculated Zn/S wt% ratio for the sample with the highest Zn content (i.e. after 100 cycles) was set to unity and the values calculated for all other films normalized accordingly (See supplementary information S1). The normalized Zn/S wt% ratio against the number of cycles, Figure 5A, clearly shows that the ZnO deposition rate increases with the number of cycles, with an initial gentle slope (up to about 50 cycles) followed by a steep one. This is in contrast to classical ALD where the mass accumulation/cycle is constant because each cycle grows a monolayer on a substrate with a contestant surface area.[38] In the case of ALD inside the polymer film, on the other hand, the first cycles lead to the nucleation of small ZnO clusters, as evident from the SEM images in Figure 4. During these first ~50 cycles the ZnO mass accumulation is slow due to the complicated kinetics of cluster nucleation. However, once particle growth is faster than particle nucleation the surface area available for ZnO increases dramatically with the number of cycles. The significant increase of surface area in each cycle leads to the observed sharp increase in the rate of ZnO mass accumulation.

The final confirmation of the growth mechanism was established by surface treating the P3HT with OH groups to allow the conventional layer-by-later ALD of ZnO on the polymer surface. Two methods for generating OH groups on the polymer surface were applied: exposure to high humidity or exposure to mild oxygen plasma. Immediately after the treatment the films were introduced to the ALD process of 75 DEZ/water cycles. The HRSEM cross section images of the post-ALD treated films are presented in Figure 5 B and C. The HRSEM images show that both pre-treatments result in ZnO growth strictly on the P3HT surface, in strong contrast to the non-treated film where the ZnO grows inside the polymer film. The P3HT/ZnO bilayers are formed because both treatments enrich the surface of the P3HT film with hydrophilic groups, either due to water adsorption in high humidity conditions or P3HT oxidation due to the plasma process. In the first DEZ cycle the DEZ reacts with the hydrophilic surface in a process similar to the conventional initial ALD process expressed in equation 3. Nucleation of ZnO on the P3HT's surface blocks the diffusion of the precursors into the film and the subsequent DEZ/water cycling leads to the self-limiting layer-by-layer ZnO film growth. It can also be noted that the ZnO layer grown on the plasma treated sample is considerably smoother than that grown on the humidity treated film due to a more homogenous distribution of the hydrophilic groups on the P3HT surface by the plasma treatment.

Finally, after establishing the ALD mechanism of ZnO in P3HT and determining the parameters for directing a hybrid BHJ morphology, we study their suitability for solar cells. Photo induced charge generation is studied using time resolved microwave photoconductivity (TRMC) which is a contact-less technique and hence allows us to follow charge generation with no effects of the contact quality. TRMC measures the change in film conductance due to photo-excited charge generation using a sensitive microwave circuitry with nanosecond time resolution. Figure 6 plots the yield of photo-induced electrons and holes (φ) and the sum of their mobilities (Σμ) as a function of photon flux for P3HT/ZnO films prepared using 0, 25, 38, 55, and 75 DEZ/water deposition cycles. For all samples the φΣμ values decrease with increasing the photon flux implying that higher order processes, such as exciton-exciton annihilation or exciton-hole recombination, are occurring[25]. We therefore compare the φΣμ values obtained for the different samples for the same photon flux. Generally, the φΣμ value increases with the number of ZnO ALD cycles. This increase is due to an increase in the number of charges and/or their mobility. Because the P3HT absorbance spectrum does not significantly change with ZnO loading (Figure 3) we assume that hole mobility is similar in all films. Accordingly, the increase of the photoconductance is attributed to two contributions: the yield of free carriers and/or the electron mobility. The similarity between the correlation of ZnO mass accumulation (Figure 5A) and TRMC signal (inset of Figure 6) with the number of cycles implies that the photoconductance is due to the growing interfacial area between the P3HT and the ZnO. The carriers are generated at the hybrid interface and hence increase of the interfacial area is directly translated to an increase in the yield of carriers. Notably, after 75 ALD cycles the photoconductance reaches a value of 8×10-3cm2/Vs, similar to that obtained for conjugated polymer/ZnO films and associated with hopping of electrons between ZnO particles.[20] Therefore, we suggest that the high photoconductance obtained for the 75-cycle ALD films also includes a contribution of an increase in electron mobility due to the large volume fraction of ZnO in the films.[24].

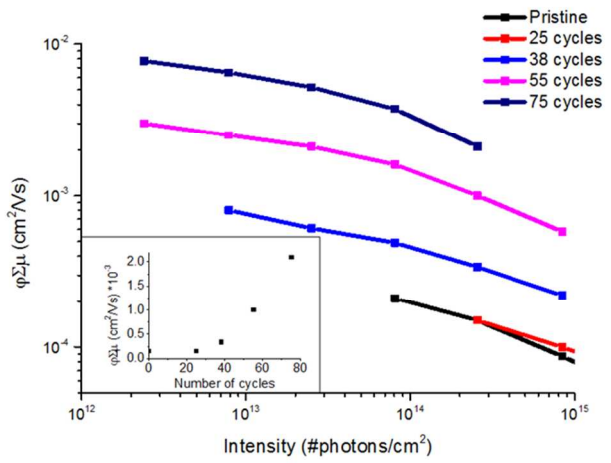

Figure 6: Product of the quantum yield per absorbed photon (φ) and the sum of the charge carrier mobilities (∑μ) versus incident intensity normalized to the optical absorption of pristine and P3HT/ZnO films after 25, 38, 55 and 75 DEZ/water ALD cycles. The inset presents the same product versus the number of ALD cycles for the 2.5×10^{14} photons/cm^2 per pulse flux measurement.

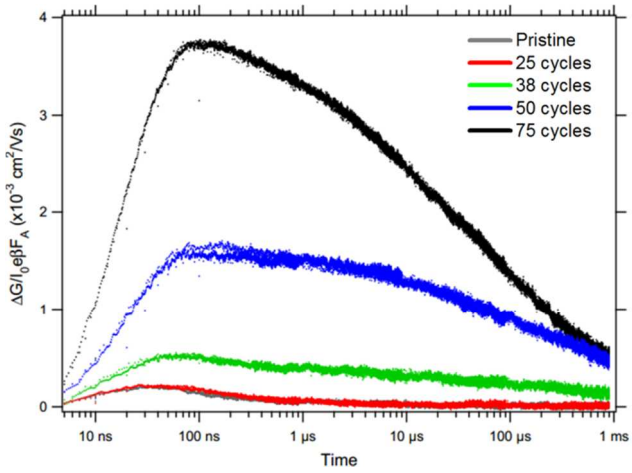

Figure 7: Intensity normalized photoconductance traces recorded for P3HT/ZnO films after 0, 25, 38, 55 and 75 DEZ/water ALD cycles. Optical excitation was done using a 3.5 ns (FWHM) laser pulse at λ = 500 nm with an incident intensity of 8×10^{13} photons/cm^2 per pulse.

Figure 7 shows the microwave photoconductivity transients of the same films. As no electrodes are used in this technique the decay of the signal is due to charge carrier recombination or mobility relaxation. Large variations in charge carrier lifetimes for the different films can be discerned. The pristine and 25-cycle films the $\tau_{1/2}$ values are approximately 0.25 μs, in good agreement with those previously reported for pristine P3HT layers[39]. However, after 38- and 55-cycles the $\tau_{1/2}$ values are dramatically higher reaching up to an extensive value of 100 μs. Interestingly, for the sample with the highest ZnO loading, i.e. after 75 cycles, the $\tau_{1/2}$ drops to 35 μs. We speculate that in the 38- and 55-cycle samples electrons are immobilized in shallow traps preventing their recombination with holes, and resulting in extensively long lifetimes. However, after 75 cycles a percolation network is formed which supports electron mobility and hence also increases the chances for recombination, effectively reducing the carrier lifetime.

Finally, the viability of ALD for processing hybrid photovoltaic films was demonstrated by integrating the P3HT/ZnO films as the active layer in devices. The solar cells had the general simple device structure: ITO/PEDOT:PSS/P3HT:ZnO/Al. The current density/voltage (J-V) curves and device parameters as a function of the number of ALD cycles are shown in Figure 8 and summarized in Table 1. The open circuit voltage (V_{oc}) of all devices is independent of the number of cycles indicating that in all cases the current is generated at the same type of interface, i.e. P3HT/ZnO. However, the short circuit current densities (J_{sc}) show a strong dependence on the number of ALD cycles. Namely, the photocurrent increases with the amount of ZnO in the film. The low photocurrents from the 25- and 38-cycles samples are in good agreement with the SEM, EDS and TRMC results that showed few, small and disconnected ZnO particles which limit the yield of free carrier generation. After 50 cycles the photocurrent rises due to an increase in the hybrid interfacial area (SEM and EDS) where more free carriers can be generated, in good agreement with the increase of the photoconductance (TRMC). A dramatic increase in J_{sc} is observed for the 75-cycle sample, showing an average value of 0.6 [mA/cm^2]. This notable rise is in good agreement with the morphological changes after 75 deposition cycles (Figure 4 E), showing that the ZnO fraction in the hybrid film is considerably higher than for the low cycles samples allowing a much higher yield of exciton to dissociation. Moreover, the ZnO clusters are significantly larger forming a pseudo-interconnected inorganic network that could support electron transport to the top contact. Another crucial morphological advantage in the 75-cycle sample is the presence of a continuous ZnO layer on top of the hybrid film. This ZnO layer acts as an electron selective interlayer at the interface with the top electrode. The optimal photovoltaic morphology obtained after 75-cycles is also evident by comparing the increase in photocurrent and photoconductance when going from 50 to 75 cycles. In contrast to photocurrent, TRMC is incapable of measuring macroscopic features such as carrier percolation[20] or contact selectivity. Hence, while the photoconductance is merely 3 times higher in the 75-cycle film compared to that in the 50-cycle film, the photocurrent is ~20 times higher. This difference demonstrates that ALD is suitable to both grow the ZnO network inside P3HT and also control the morphology to suit the prerequisites of photovoltaic films. Indeed, the best 75-cycles device showed a V_{oc} of 0.46 V, J_{sc} of 0.9 mA/cm^2 and power conversion efficiency (PCE) of 0.12%. These results, although lower than best preforming hybrid ZnO/P3HT devices, are of the same magnitude as many previous reports on similar photovoltaic systems, demonstrating the feasibility of ALD as a processing technique for hybrid solar cells.[18, 40, 41]

Table 1. Summary of device performance parameters as a function of the number of ALD cycles. Measurements are averaged over 24 devices for each deposition.

ALD cycles	V_{oc} (V)	J_{sc} (mA/cm^2)	FF (%)	PCE (%)
0	0.3 ± 0.04	3.8×10^{-3} ± 0.5×10^{-3}	39±1	4×10^{-4} ± 1×10^{-4}
25	0.28 ± 0.04	4.6×10^{-3} ± 0.6×10^{-3}	37±1	5×10^{-4} ± 1×10^{-4}
38	0.31 ± 0.03	6.4×10^{-3} ± 0.8×10^{-3}	36±1	8×10^{-4} ± 1×10^{-4}
50	0.27 ± 0.06	3.2×10^{-2} ± 8×10^{-3}	38±1	3×10^{-3} ± 6×10^{-4}
75	0.35 ± 0.05	0.6 ± 0.1	37±1	0.11 ± 0.02

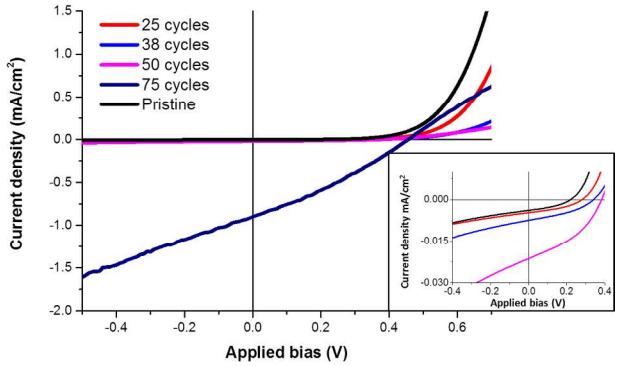

Figure 8: Representative photocurrent density-voltage characteristics (J-V) under 1.5AM illumination of the different deposition samples. Black- pristine P3HT, red- 25 deposition cycles, blue- 38, magenta- 50, navy- 75. The inset is an expansion of a selected area of the figure.

Conclusions

In summary, we have showed that ALD of ZnO into pristine P3HT films from DEZ and water precursors is a viable and simple processing technique for the formation of hybrid organic/inorganic BHJs. The BHJ was formed by diffusion of the DEZ precursor into the amorphous regions of the P3HT, followed by *in-situ* poly-condensation of ZnO nano-crystals dispersed inside the film. Importantly, we confirmed that P3HT order and its optical properties were not impaired during the ALD sequence. The ZnO mass accumulation and its morphology inside the organic film as a function of the number of ALD cycles was followed and suggested a two-step nucleation and growth mechanism. By judicious selection of the deposition parameters we were able to generate the optimal BHJ photovoltaic morphology: high organic/inorganic interfacial area, interconnected ZnO/P3HT networks and a capping electron transporting layer. Indeed, the photovoltaic devices comprising the simply processed ALD films showed promising performances. We believe that optimization of the deposition parameters could lead to further improvement of the photovoltaic performance and show significantly higher PCE. In addition to demonstrating that ALD is suitable and useful for the fabrication of HOPVs, this study establishes a general new approach: harnessing the diffusion of small molecules, such as additives or precursors, into pre-formed organic films (similar ZnO penetration was observed in MEH-PPV films, see supplementary information S2) to direct morphologies and functionalities that are complicated to achieve or even unattainable in conventional methods.

Acknowledgements

This research was partially supported by the Israeli Nanotechnology Focal Technology Area project on "Nanophotonics and Detection" and the Helmsley Alternative Energy series of the Technion, Israel Institute of Technology, and the Weizmann Institute of Science

Notes and references

[a] Department of Materials Science and Engineering, Technion, Israel Institute of Technology, Haifa, 32000 Israel.
[b] Russel Berrie Nanotechnology Institute, Technion, Israel Institute of Technology, Haifa, 32000 Israel.
[c] Department of Chemical Engineering, Delft University of Technology, Delft, The Netherlands

Electronic Supplementary Information (ESI) available: See DOI: 10.1039/b000000x/

1. L. Dou, J. You, Z. Hong, Z. Xu, G. Li, R. A. Street and Y. Yang, *Advanced Materials*, 2013, **25**, 6642-6671.
2. B. Kippelen and J.-L. Bredas, *Energy & Environmental Science*, 2009, **2**, 251-261.
3. F. Liu, Y. Gu, X. Shen, S. Ferdous, H.-W. Wang and T. P. Russell, *Progress in Polymer Science*, 2013, **38**, 1990-2052.
4. J. Jo, S.-I. Na, S.-S. Kim, T.-W. Lee, Y. Chung, S.-J. Kang, D. Vak and D.-Y. Kim, *Advanced Functional Materials*, 2009, **19**, 2398-2406.
5. A. C. Mayer, M. F. Toney, S. R. Scully, J. Rivnay, C. J. Brabec, M. Scharber, M. Koppe, M. Heeney, I. McCulloch and M. D. McGehee, *Advanced Functional Materials*, 2009, **19**, 1173-1179.
6. M. Wright and A. Uddin, *Solar Energy Materials and Solar Cells*, 2012, **107**, 87-111.
7. P. A. Van Hal, M. M. Wienk, J. M. Kroon, W. J. H. Verhees, L. H. Slooff, W. J. H. Van Gennip, P. Jonkheijm and R. A. J. Janssen, *Advanced Materials*, 2003, **15**, 118-121.
8. T. Segal-Peretz, O. Leman, A. M. Nardes and G. L. Frey, *Journal of Physical Chemistry C*, 2012, **116**, 2024-2032.
9. A. L. Briseno, T. W. Holcombe, A. I. Boukai, E. C. Garnett, S. W. Shelton, J. J. M. Fréchet and P. Yang, *Nano Letters*, 2009, **10**, 334-340.
10. W. J. E. Beek, M. M. Wienk and R. A. J. Janssen, *Advanced Materials*, 2004, **16**, 1009-1013.
11. L. E. Greene, M. Law, B. D. Yuhas and P. Yang, *The Journal of Physical Chemistry C*, 2007, **111**, 18451-18456.
12. T.-W. Zeng, Y.-Y. Lin, H.-H. Lo, C.-W. Chen, C.-H. Chen, S.-C. Liou, H.-Y. Huang and W.-F. Su, *Nanotechnology*, 2006, **17**, 5387.
13. K. M. Coakley and M. D. McGehee, *Applied Physics Letters*, 2003, **83**, 3380-3382.
14. P. Ravirajan, A. M. Peiró, M. K. Nazeeruddin, M. Graetzel, D. D. C. Bradley, J. R. Durrant and J. Nelson, *The Journal of Physical Chemistry B*, 2006, **110**, 7635-7639.
15. S. D. Oosterhout, M. M. Wienk, S. S. van Bavel, R. Thiedmann, L. Jan Anton Koster, J. Gilot, J. Loos, V. Schmidt and R. A. J. Janssen, *Nat Mater*, 2009, **8**, 818-824.
16. S. M. George, *Chemical Reviews*, 2010, **110**, 111-131.
17. M. Leskelä and M. Ritala, *Thin Solid Films*, 2002, **409**, 138-146.
18. R. Saberi Moghaddam, S. Huettner, Y. Vaynzof, C. Ducati, G. Divitini, R. H. Lohwasser, K. P. Musselman, A. Sepe, M. R. J. Scherer, M. Thelakkat, U. Steiner and R. H. Friend, *Nano Letters*, 2013, **13**, 4499-4504.
19. C. A. Wilson, R. K. Grubbs and S. M. George, *Chemistry of Materials*, 2005, **17**, 5625-5634.
20. P. A. C. Quist, W. J. E. Beek, M. M. Wienk, R. A. J. Janssen, T. J. Savenije and L. D. A. Siebbeles, *Journal of Physical Chemistry B*, 2006, **110**, 10315-10321.
21. S. D. Chavhan, R. D. Abellon, A. J. J. M. Van Breemen, M. M. Koetse, J. Sweelssen and T. J. Savenije, *Journal of Physical Chemistry C*, 2010, **114**, 19496-19502.
22. T. J. Savenije, D. H. K. Murthy, M. Gunz, J. Gorenflot, L. D. A. Siebbeles, V. Dyakonov and C. Deibel, *Journal of Physical Chemistry Letters*, 2011, **2**, 1368-1371.
23. D. H. K. Murthy, A. Melianas, Z. Tang, G. Juška, K. Arlauskas, F. Zhang, L. D. A. Siebbeles, O. Inganäs and T. J. Savenije, *Advanced Functional Materials*, 2013, **23**, 4262-4268.
24. D. C. Olson, Y. J. Lee, M. S. White, N. Kopidakis, S. E. Shaheen, D. S. Ginley, J. A. Voigt and J. W. P. Hsu, *Journal of Physical Chemistry C*, 2008, **112**, 9544-9547.

25. T. J. Savenije, A. J. Ferguson, N. Kopidakis and G. Rumbles, *Journal of Physical Chemistry C*, 2013, **117**, 24085-24103.
26. E. Guziewicz, I. A. Kowalik, M. Godlewski, K. Kopalko, V. Osinniy, A. Wójcik, S. Yatsunenko, E. Łusakowska, W. Paszkowicz and M. Guziewicz, *Journal of Applied Physics*, 2008, **103**, 033515.
27. H. McMurdie, M. Morris, E. Evans, B. Paretzkin, W. Wong-Ng, L. Ettlinger and C. Hubbard, *Powder Diffraction*, 1986, **1**, 76.
28. M. Yasaka, *The Rigaku Journal*, 2010, **26**.
29. V. Srikant and D. R. Clarke, *Journal of Applied Physics*, 1998, **83**, 5447-5451.
30. T. J. Savenije, J. E. Kroeze, X. Yang and J. Loos, *Thin Solid Films*, 2006, **511-512**, 2-6.
31. V. Shrotriya, J. Ouyang, R. J. Tseng, G. Li and Y. Yang, *Chemical Physics Letters*, 2005, **411**, 138-143.
32. W. J. D. Beenken and T. Pullerits, *Journal of Physical Chemistry B*, 2004, **108**, 6164-6169.
33. P. Swee-Yong, C. Kwang-Leong, H. Xianghui and S. Chongxin, *Nanotechnology*, 2008, **19**, 435609.
34. I. Dekman, R. Brener and G. L. Frey, *Journal of Materials Chemistry C*, 2013, **1**, 6522-6525.
35. Y. Zilberman, R. Ionescu, X. Feng, K. Müllen and H. Haick, *ACS Nano*, 2011, **5**, 6743-6753.
36. H. E. Katz and J. Huang, *Annual Review of Materials Research*, 2009, **39**, 71-92.
37. Z.-K. Tan, Y. Vaynzof, D. Credgington, C. Li, M. T. L. Casford, A. Sepe, S. Huettner, M. Nikolka, F. Paulus, L. Yang, H. Sirringhaus, N. C. Greenham and R. H. Friend, *Advanced Functional Materials*, 2014, **24**, 3051-3058.
38. J. A. Libera, J. W. Elam and M. J. Pellin, *Thin Solid Films*, 2008, **516**, 6158-6166.
39. G. Dicker, M. P. de Haas, L. D. A. Siebbeles and J. M. Warman, *Physical Review B*, 2004, **70**, 045203.
40. I. Gonzalez-Valls and M. Lira-Cantu, *Energy & Environmental Science*, 2009, **2**, 19-34.
41. K. P. Musselman, S. Albert-Seifried, R. L. Z. Hoye, A. Sadhanala, D. Muñoz-Rojas, J. L. Macmanus-Driscoll and R. H. Friend, *Advanced Functional Materials*, 2014, **24**, 3562-3570.

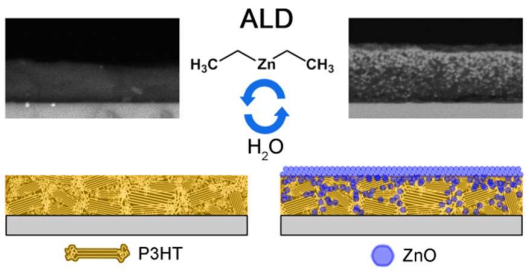

ALD ZnO precursors diffuse into the disordered regions of a P3HT film yielding the bulk heterojunction morphology for hybrid photovoltaics